Journal of Molecular Cell Biology (2023), 15(6), mjad041 https://doi.org/10.1093/jmcb/mjad041
Published online June 26, 2023

Article

Dynamic phosphorylation of CENP-N by CDK1 guides accurate chromosome segregation in mitosis

Ran Liu[1,2,†], Zhen Dou[1,2,†], Tian Tian[1,†], Xinjiao Gao[1,2], Lili Chen[1], Xiao Yuan[1,2], Chunyue Wang[1], Jiahe Hao[1], Ping Gui[1,2,3], McKay Mullen[1,3], Felix Aikhionbare[3], Liwen Niu[1,2], Guoqiang Bi[1,2], Peng Zou[4], Xuan Zhang[1], Chuanhai Fu[1,2], Xuebiao Yao[1,2], Jianye Zang[1,*], and Xing Liu[1,2,*]

[1] MOE Key Laboratory for Cellular Dynamics & Hefei National Research Center for Interdisciplinary Sciences at the Microscale, University of Science and Technology of China School of Life Sciences, Hefei 230026, China
[2] CAS Center for Excellence in Molecular and Cell Sciences, Anhui Key Laboratory for Cellular Dynamics and Chemical Biology, Hefei 230027, China
[3] Keck Center for Cellular Dynamics, Morehouse School of Medicine, Atlanta, GA 30310, USA
[4] College of Chemistry and Molecular Engineering, Peking University, Beijing 100871, China
[†] These authors contributed equally to this work.
[*] Correspondence to: Jianye Zang, E-mail: zangjy@ustc.edu.cn; Xing Liu, E-mail: xing1017@ustc.edu.cn

Edited by Zhiyuan Shen

In mitosis, accurate chromosome segregation depends on the kinetochore, a supermolecular machinery that couples dynamic spindle microtubules to centromeric chromatin. However, the structure–activity relationship of the constitutive centromere-associated network (CCAN) during mitosis remains uncharacterized. Building on our recent cryo-electron microscopic analyses of human CCAN structure, we investigated how dynamic phosphorylation of human CENP-N regulates accurate chromosome segregation. Our mass spectrometric analyses revealed mitotic phosphorylation of CENP-N by CDK1, which modulates the CENP-L–CENP-N interaction for accurate chromosome segregation and CCAN organization. Perturbation of CENP-N phosphorylation is shown to prevent proper chromosome alignment and activate the spindle assembly checkpoint. These analyses provide mechanistic insight into a previously undefined link between the centromere–kinetochore network and accurate chromosome segregation.

Keywords: mitosis, centromere, CENP-N, CDK1, phosphorylation

Introduction

The kinetochore is a supermolecular complex assembled at each centromere in eukaryotes. It provides a chromosomal attachment point for the mitotic spindle, linking the chromosome to microtubules, and functions in initiating, controlling, and monitoring the movements of chromosomes during mitosis (Cleveland et al., 2003; Liu et al., 2020). The kinetochore of animal cells contains two functional domains: the inner kinetochore, which is tightly and persistently associated with centromeric DNA sequences throughout the cell cycle, and the outer kinetochore, which is composed of many dynamic protein complexes that interact with microtubules only during mitosis (McKinley and Cheeseman, 2016). The centromere is built on a specific foundation called the CENP-A nucleosome and the constitutive centromere-associated network (CCAN). CCAN contains 16 subunits, which form one of the major complexes in the kinetochore (Foltz et al., 2006; Okada et al., 2006; Hori et al., 2008). CENP-C and CENP-T, two CCAN subunits, provide a platform for the assembly of the outer layer of kinetochores (Hori et al., 2008; Schleiffer et al., 2012). The outer kinetochore also comprises three subcomplexes, KNL1, MIS12, and NDC80, which are collectively referred to as the KMN network (Cheeseman and Desai, 2008). CCAN is associated with centromeric chromatin, and the KMN network binds directly to spindle microtubules. Through its NDC80 subcomplex, the KMN network provides a site for accurate segregation of chromosomes in daughter cells (Cheeseman and Desai, 2008; Musacchio and Desai, 2017).

Received July 26, 2022. Revised January 9, 2023. Accepted June 24, 2023.

Mitosis is orchestrated by signaling cascades that coordinate mitotic processes and ensure accurate chromosome segregation. The key switch for the onset of mitosis is the archetypal cyclin-dependent kinase (CDK1). In addition to the master mitotic kinase CDK1, three other protein serine/threonine kinase families, including Polo kinases, Aurora kinases, and NEK kinases, are involved (Dou et al., 2019). Early electron microscopic (EM) analyses indicated that the outer kinetochore structure changes dynamically during mitotic progression (Yao et al., 1997). However, it remains elusive how the kinetochore structure is reorganized to orchestrate dynamic interactions between spindle microtubules and chromosomes.

Recognition of CENP-A-containing chromatin by CENP-N, a CCAN subunit, is a critical step in the assembly of functional kinetochore at the centromere to enable accurate chromosome segregation during cell division (Carroll et al., 2009). CENP-N is recruited to centromeres during the S phase and gradually dissociates during the G2 phase (Hellwig et al., 2011). This dynamic assembly of CENP-N onto the centromere is regulated by changed accessibility of CENP-N to the RG loop of CENP-A (Arg80/Gly81) during the compacting–opening transition of centromeric chromatin structure through the cell cycle (Fang et al., 2015). Our recent cryo-EM analyses indicated that CENP-L and CENP-N, two CCAN subunits, form a channel-like structure that binds to DNA (Tian et al., 2022). We consolidate the structural analyses of CCAN with the biochemical characterization of CDK1-elicited phosphorylation of CENP-N. Our structural–functional analyses revealed a surprising link between the binding of CENP-L–CENP-N to centromeric DNA and the structural dynamics of CCAN reorganization during mitotic chromosome alignment.

Results

The CENP-L–CENP-N heterodimer organizes CCAN integrity

Our cryo-EM analyses of CCAN revealed that CENP-L–CENP-N forms a channel-like structure (Tian et al., 2022). To assess the importance of CENP-L–CENP-N channel activity in CCAN assembly, we engineered a membrane-permeable peptide (TAT-CENP-N$^{271-300}$) that contains a CENP-N binding interface to CENP-L (Figure 1A) and used this peptide to interrogate endogenous interaction between CENP-L and CENP-N as previously reported (McKinley et al., 2015). As shown in Figure 1B, the addition of TAT-CENP-N$^{271-300}$ into HeLa cells disrupted the formation of endogenous CENP-L–CENP-N complex (hereafter referred to as the CENP-LN complex), as judged by an immunoprecipitation assay, indicating that the peptide is a useful tool for interrogating CENP-LN complex activity. We next sought to test whether treatment of HeLa cells in S and G2 phases with TAT-CENP-N$^{271-300}$ alters cell cycle progression into mitosis. Real-time imaging indicated that compared with the control scramble peptide treatment (Figure 1C, top panel), TAT-CENP-N$^{271-300}$ treatment perturbed chromosome segregation and prevented mitotic entry (Figure 1C, arrows in the bottom panel). Statistical analyses confirmed that TAT-CENP-N$^{271-300}$ treatment resulted in chromosome segregation defects (Figure 1D). Thus, the association of CENP-L with CENP-N is essential for accurate chromosome segregation in mitosis.

Electrostatic interactions organize the association of CENP-L with CENP-N

Post-translational modifications govern mitotic progression via kinetochore–microtubule interactions (Cleveland et al., 2003; McKinley and Cheeseman, 2016; Hara et al., 2018). Structural analyses and sequence alignment revealed four evolutionarily conserved potential phosphorylation sites of CENP-N (Thr273, Ser298, Ser299, and Ser320) at the interface between CENP-L and CENP-N. Two of these sites, Ser299 and Ser320, are highly conserved, conform to CDK phosphorylation consensus motifs, and are surrounded by other conserved residues (Figure 2A; Supplementary Figure S1A and B). Detailed annotation was made for adjacent amino acids surrounding Thr273, Ser299, and Ser320 (Figure 2A). To determine whether electrostatic charges on these sites modulate CENP-L–CENP-N interactions, we carried out mutagenesis to mimic non-phosphorylatable CENP-N and site-specific phosphorylation of CENP-N (T273A/D, S299A/D, and S320A/D). Western blotting analyses showed that the protein stabilities of these six phosphophorylation mutants of CENP-N were not altered (Figure 2B). Then, we carried out immunofluorescence microscopic analyses of HeLa cells expressing these mutants. As shown in Figure 2C, the phospho-mimicking CENP-N S299D exhibited reduced levels of kinetochore localization, while wild-type CENP-N and CENP-N S299A were stably localized to kinetochores. CENP-N T273A/D mutants also resulted in an apparent reduction in their centromere localization (Figure 2C). Although Ser320 is predicted to be a potential phosphorylation site of CENP-N, the phosphorylation-mimicking mutant S320D did not alter its centromere localization (Figure 2C). Quantitative analyses confirmed that the fluorescence intensities of the T273A/D and S299D mutants at the centromere were significantly reduced (Figure 2D). We next assessed whether phosphorylation of these sites regulates the interaction of CENP-N with CENP-L. As shown in Figure 2B, phospho-mimicking CENP-N S299D failed to bind to CENP-L, while the binding of wild-type CENP-N or non-phosphorylatable CENP-N S299A to CENP-L was not affected, suggesting that the CENP-L–CENP-N association is regulated by phosphorylation of CENP-N Ser299. To clarify whether CENP-LN complex formation influences the ability of CENP-N to interact with CENP-A, we carried out a co-immunoprecipitation assay using CENP-N phosphorylation mutants. As a result, both CENP-N S299A and CENP-N S299D exhibited comparable binding to CENP-A as wild-type CENP-N, indicating that phosphorylation of C-terminal CENP-N does not affect the binding of CENP-N to CENP-A (Supplementary Figure S1C). Consistent with their kinetochore localization, CENP-N T273A/D reduced their interactions with CENP-L, whereas CENP-N S320A/D remained bound to CENP-L (Figure 2B). Thus, the association of CENP-L with CENP-N consists of multivalent interactions, and mitotic phosphorylation may regulate CENP-LN complex remodeling.

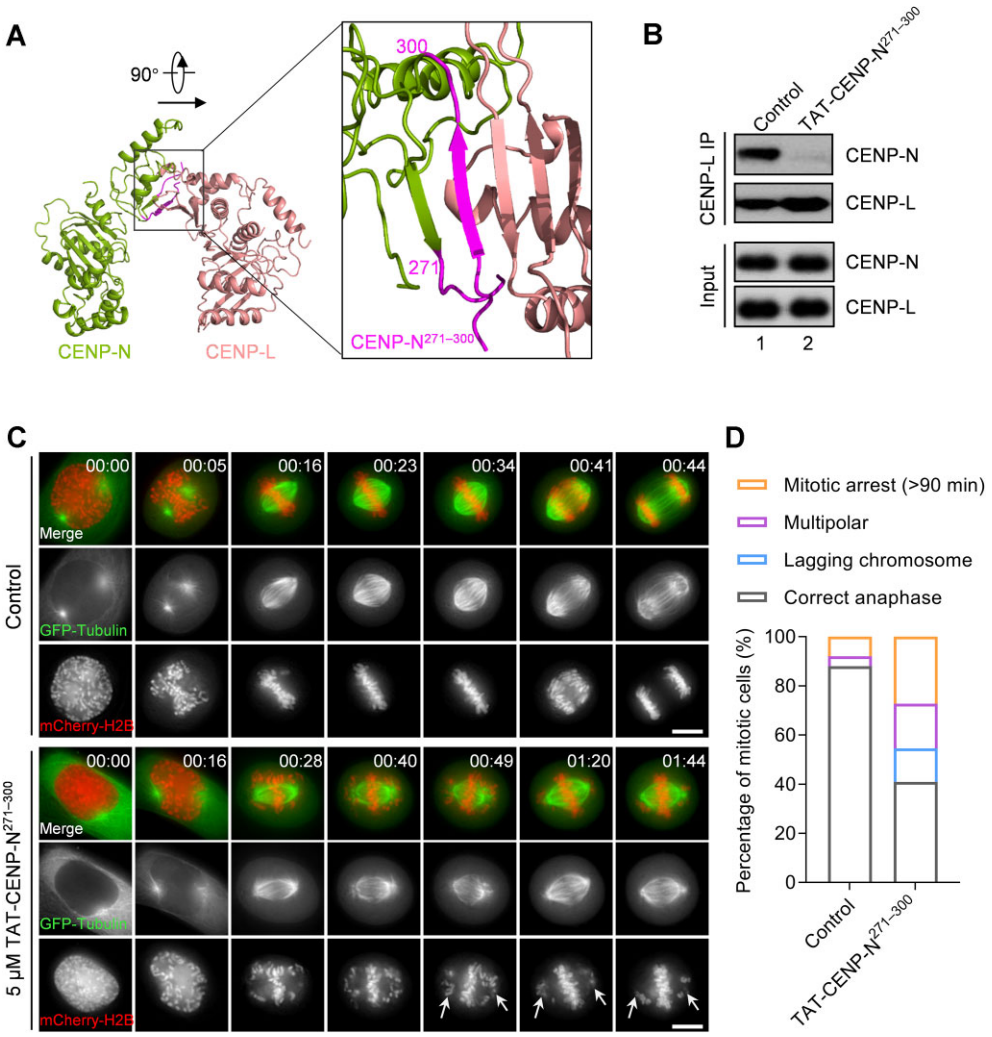

Figure 1 The interaction between CENP-L and CENP-N is required for accurate mitotic progression. (**A**) The binding interface between CENP-L and CENP-N. A close-up view of the key β-strand of CENP-N at the CENP-L–CENP-N interface is shown in magenta. (**B**) Immunoprecipitation analyses show that the TAT-CENP-N$^{271–300}$ peptide disrupts the interaction between CENP-L and CENP-N. (**C**) Disrupting the CENP-L–CENP-N interaction causes chromosome misalignment. Representative images illustrating mitotic progression in mCherry-H2B-expressing cells treated with scramble control peptide or 5 μM TAT-CENP-N$^{271–300}$ peptide in Opti-MEM for 60 min. Live cell imaging analyses were performed under a DeltaVision microscope. Images were acquired at the indicated time points after the start of nuclear envelope breakdown (control: $n = 25$, TAT-CENP-N$^{271–300}$: $n = 34$). Scale bar, 10 μm. (**D**) Bar graphs illustrating the percentages of various phenotypes of cells treated as in **C**.

CENP-N is a bona fide substrate of CDK1

We carried out mass spectrometric analyses of CENP-N isolated from mitotic HeLa cells, and the results revealed that CENP-N Ser299 is characteristically phosphorylated (Figure 3A; Supplementary Figure S2A and B). To determine whether Ser299 is a *bona fide* substrate of CDK1, we performed *in vitro* phosphorylation assays using 3× FLAG-CENP-N proteins isolated from HEK293T cells. As shown in Figure 3B, both wild-type and Ser299-mutated CENP-N (S299A) migrated at the predicted position of ∼41 kDa (middle panel). Incubation with [γ-^{32}P]-ATP and CDK1 resulted in the incorporation of ^{32}P into wild-type CENP-N but not into the S299A mutant (Figure 3B, top panel, lanes 2 and 3). Moreover, no phosphorylation of Ser299 was evident upon incubation of wild-type CENP-N with [γ-^{32}P]-ATP and CDK1 in the presence of the CDK1 inhibitor Ro3306 (Figure 3B, lane 1). Using a phospho-Ser299 (pS299) site-specific antibody (Supplementary Figure S2C and D), we confirmed that CENP-N Ser299 is a cognate substrate of CDK1 (Figure 3B, bottom panel, lane 2).

To assess the temporal dynamics of CENP-N Ser299 phosphorylation throughout the cell cycle, we collected synchronized HeLa cells at the indicated intervals after release from the G1/S boundary and conducted immunoblotting with the pS299 antibody (Figure 3C). Cyclin B1 accumulation (6 h after release) marked the advance into the G2 phase and was sustained until anaphase onset (∼11 h after release). The temporal dynamics of CENP-N Ser299 phosphorylation were similar to those of Cyclin B1 (11 h after release, Figure 3C),

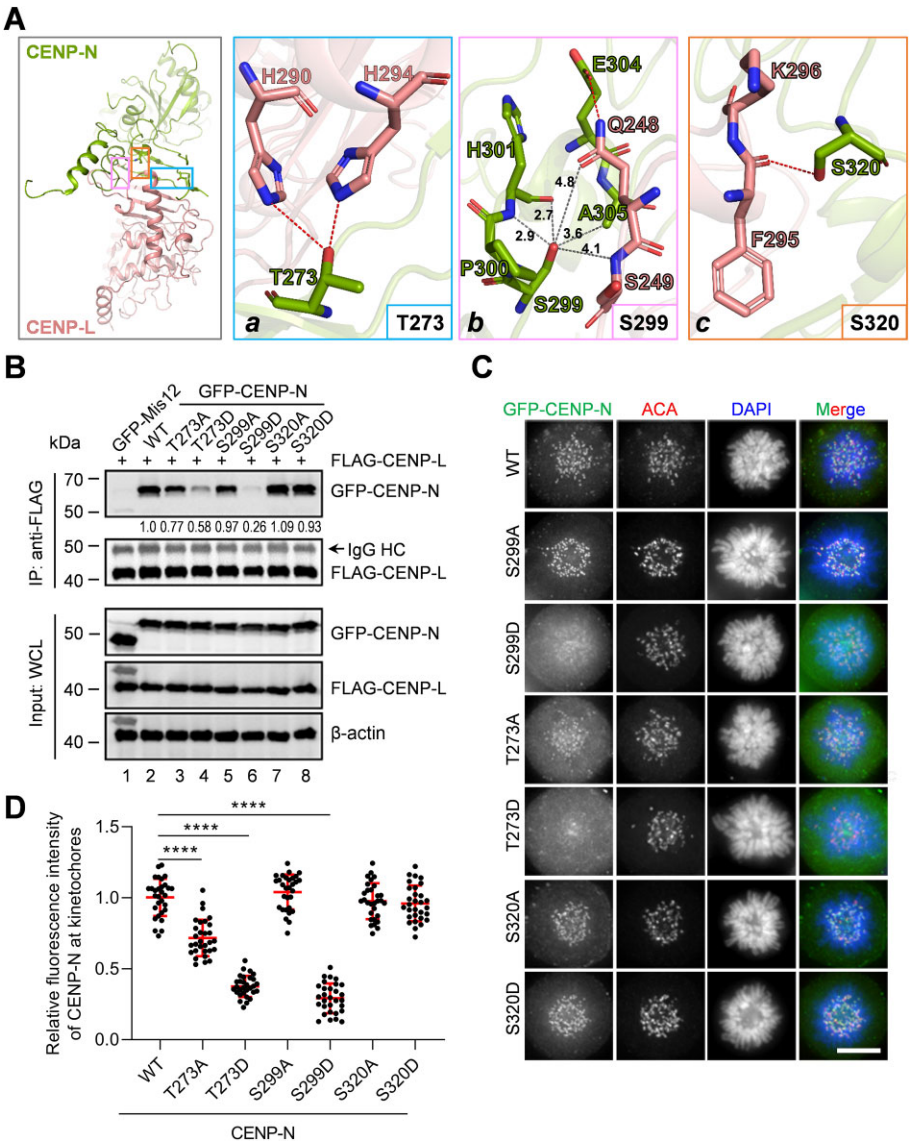

Figure 2 Analysis of potential phosphorylation sites at the CENP-L–CENP-N interface. (**A**) The overall structure of the CENP-L–CENP-N heterodimer with three residues that may be phosphorylated (Thr273, Ser299, and Ser320 labelled by different colored boxes). The enlarged view shows details of the interaction between CENP-L and CENP-N at Thr273, Ser299, and Ser320, respectively. Hydrogen bonds are indicated by red dashed lines. The gray dashed lines mark the distance between the hydroxyl group of Ser299 and its neighboring residues. (**B**) HEK293T cells were co-transfected with FLAG-CENP-L and wild-type GFP-CENP-N or different GFP-CENP-N mutants as indicated. GFP-Mis12 served as a negative control. After 24 h, the cells were collected and lysed, and immunoprecipitation was carried out using anti-FLAG M2 beads. Immunoprecipitation samples were examined by western blotting using anti-GFP, anti-FLAG, and anti-β-actin antibodies, respectively. WCL, whole-cell lysate. (**C**) Representative immunofluorescence images of cells expressing wild-type GFP-CENP-N or different GFP-CENP-N mutants as indicated. Cells were treated with S-trityl-L-cysteine, an EG5 inhibitor, for 4 h and then fixed and stained for ACA (red) and DNA (blue). Scale bar, 10 μm. ACA, anti-centromere antibody. (**D**) Bar graph illustrating the relative fluorescence intensity of CENP-N in cells treated as in **C**. Bars represent the mean kinetochore intensity (± standard deviation) normalized to the values of the GFP-CENP-N wild-type group. Each dot represents one cell (>30 cells from three independent experiments). Student's *t*-test was used to calculate *P*-values. ****$P < 0.0001$.

demonstrating that Ser299 phosphorylation is temporally regulated by CDK1–Cyclin B1. Next, we examined the subcellular distribution of phosphorylated CENP-N in asynchronized HeLa cells. As shown in Figure 3D, phosphorylated CENP-N was localized adjacent to the centromere in prometaphase cells (top panel), which was diminished as chromosomes aligned at the equator achieved in metaphase cells (bottom panel), suggesting that CDK1-mediated phosphorylation promotes CENP-N dynamics and potential reorganization of CCAN during cell cycle progression. Since Ser299 lies at the interface between CENP-L

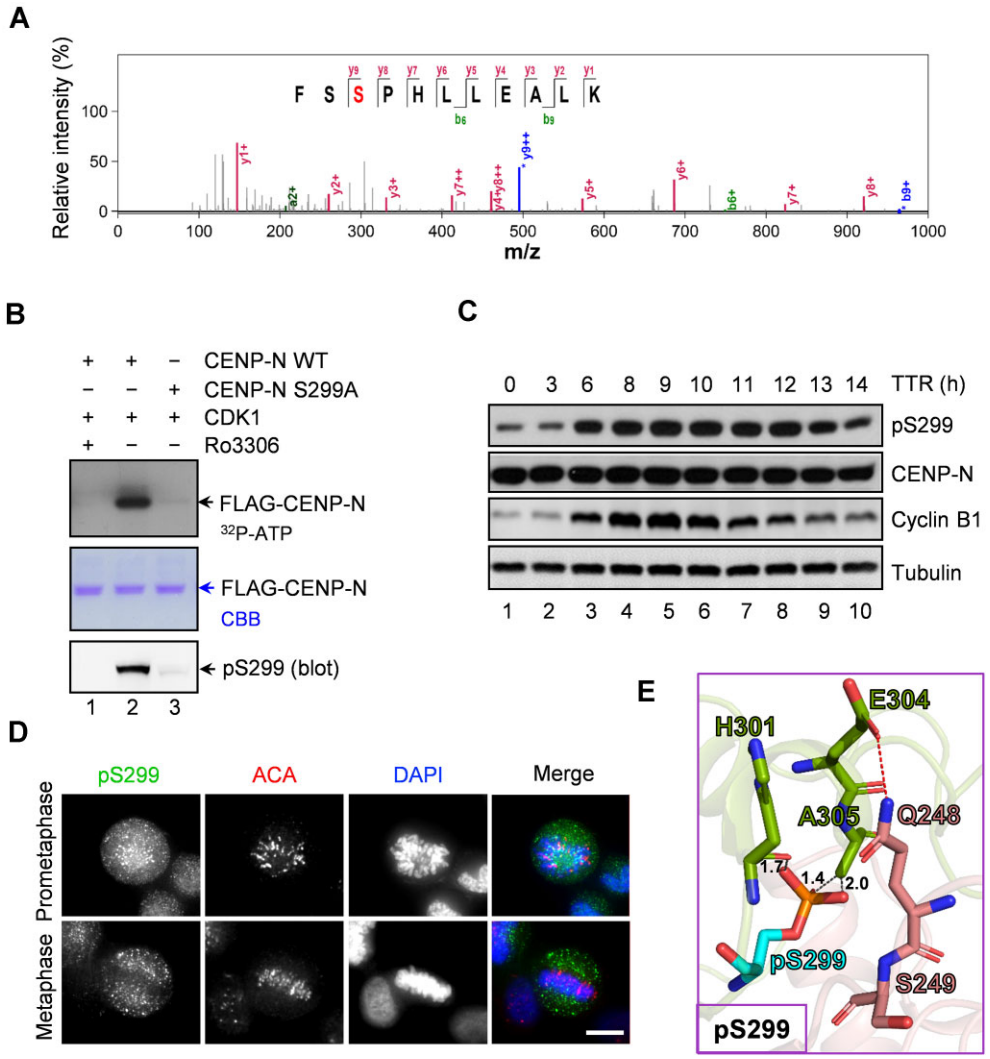

Figure 3 CENP-N is a novel physiological substrate of CDK1. (**A**) Mass spectrum of phosphorylation sites of CENP-N in mitotic cells. FLAG-CENP-N was isolated from mitotic HeLa lysates by immunoprecipitation. After extensive washes, the beads were subjected to mass spectrometric analyses. (**B**) *In vitro* phosphorylation of recombinant 3× FLAG-tagged wild-type CENP-N or CENP-N S299A by CDK1 in the absence or presence of the CDK1 inhibitor Ro3306. The upper panel shows the result of autoradiography; the middle panel shows CBB staining of the gel; and the lower panel shows the result of western blotting probed with anti-CENP-N pS299 antibody. (**C**) Temporal profile of CENP-N Ser299 phosphorylation during the cell cycle. HeLa cells were synchronized by a double thymidine block and then released and collected at the selected time points. Cell lysate samples were resolved by sodium dodecyl sulfate–polyacrylamide gel electrophoresis (SDS–PAGE) and analyzed by western blotting using anti-CENP-N pS299, anti-CENP-N, anti-Cyclin B1, and anti-tubulin antibodies, respectively. TTR, double thymidine release. (**D**) Immunofluorescence staining for pS299 of CENP-N, ACA, and DNA in prometaphase or metaphase HeLa cells. Note that the pS299 signal is strong at the prometaphase centromere but diminished in metaphase cells. Scale bar, 10 μm. (**E**) An enlarged view of the intricate CENP-L–CENP-N interface in the aftermath of phosphorylation at CENP-N Ser299. Noticeable red dashed lines signify the hydrogen bonds, while the gray dashed lines depict the distance between the phosphate group on Ser299 and other surrounding atoms that could lead to potential conflicts.

and CENP-N, we carried out molecular modeling of the CENP-L–CENP-N interface simulated based on recently resolved 3D structure of CCAN (Tian et al., 2022). Our molecular modeling analyses suggest that phosphorylation of CENP-N Ser299 could result in an allosteric change in CENP-N C-terminus due to possible repulsion extended to His301 and Ala305 (Figure 3E), which liberates the interaction of CENP-N with CENP-L in response to local CDK1 kinase activity.

Dynamic CENP-N phosphorylation regulates accurate chromosome segregation

To determine whether and how phosphorylation of CENP-N regulates chromosome segregation, we expressed wild-type CENP-N, CENP-N S299A, and CENP-N S299D constructs in HeLa cells depleted of endogenous CENP-N. Western blotting analyses showed exogenously expressed CENP-N proteins at comparable levels, ~6-fold higher than residual endogenous CENP-N

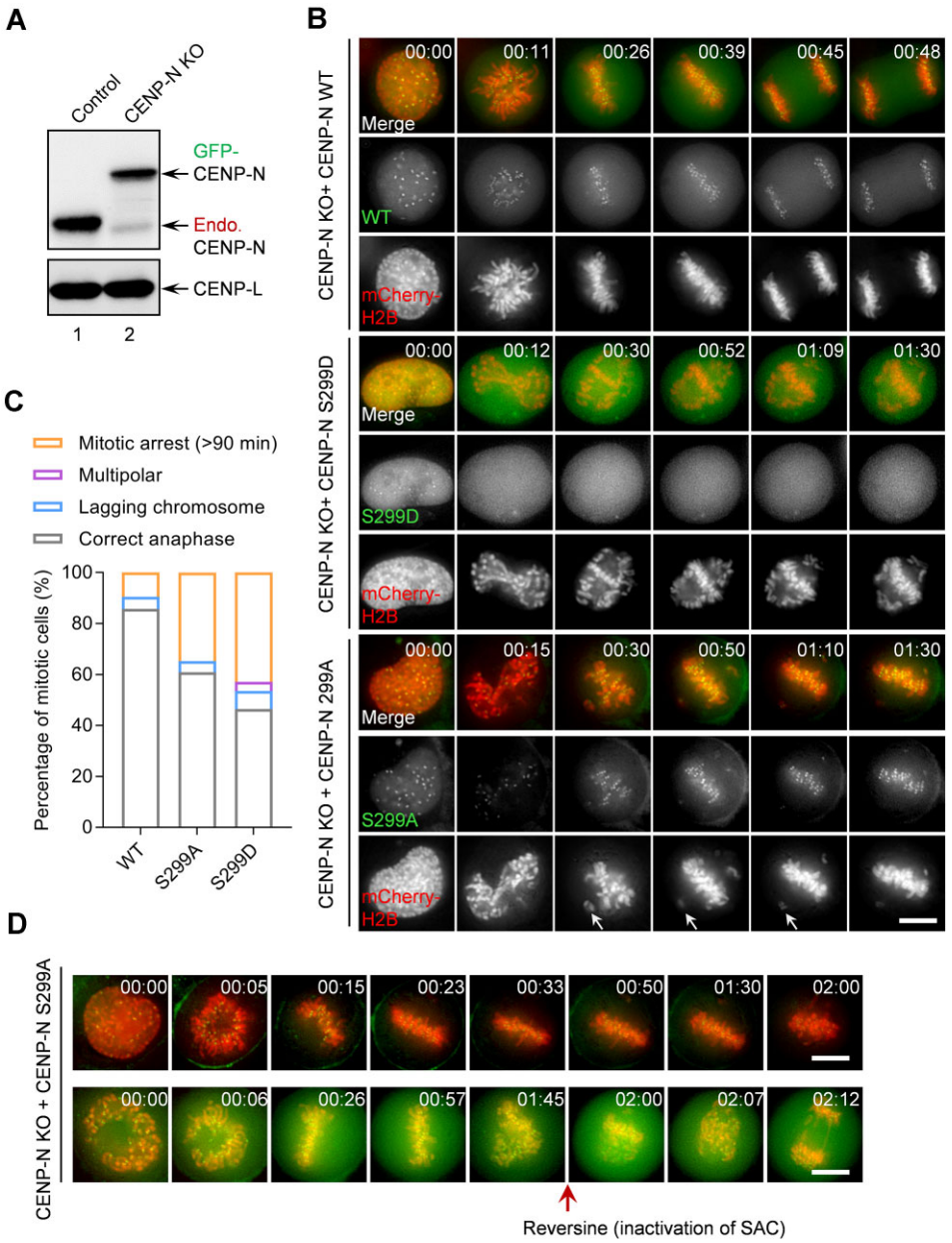

Figure 4 Perturbation of CENP-N phosphorylation impairs CCAN mechano-sensitivity. (**A**) Inducible CRISPR/Cas9-mediated endogenous CENP-N knockout HeLa cells were infected with lentiviruses expressing sgRNA-resistant GFP-tagged CENP-N protein. Western blotting analysis was performed to evaluate the endogenous and exogenous CENP-N protein levels. KO, knockout. (**B**) Real-time imaging of endogenous CENP-N knockout HeLa cells expressing GFP-tagged wild-type CENP-N or GFP-tagged CENP-N mutants. Note that both S299A and S299D cause mitotic arrest with chromosome alignment defects. Chromosomes are marked by mCherry-H2B. Scale bar, 10 μm. (**C**) Quantification of mitotic phenotypes in cells treated as in **B**. Approximately 50 cells were counted for each group. (**D**) Real-time imaging of endogenous CENP-N knockout HeLa cells expressing the non-phosphorylatable CENP-N S299A mutant. S299A-caused mitotic arrest activates the spindle assembly checkpoint. The addition of reversine releases the spindle assembly checkpoint and mitotic blockage. Chromosomes are marked by mCherry-H2B. SAC, spindle assembly checkpoint. Scale bar, 10 μm.

(Figure 4A). Real-time imaging analyses showed that cells expressing wild-type CENP-N achieved metaphase chromosomal alignment within ∼30 min after nuclear envelope breakdown and subsequently progressed into anaphase onset, which rescued the phenotype of CENP-N suppression (Figure 4B, top panel). Cells expressing phospho-mimicking CENP-N S299D failed to achieve metaphase alignment, even at 90 min after nuclear envelope breakdown, consistent with the disruption of the CENP-L–CENP-N interaction (Figure 4B, middle panel). Thus, persistent phosphorylation inhibits the formation

of the functional CENP-L–CENP-N channel, which is essential for accurate chromosome segregation. Interestingly, although CENP-N S299A remained bound to the kinetochore and associated with CENP-L, persistent expression of CENP-N S299A perturbed chromosome alignment at the equator (Figure 4B, bottom panel). These cells spent much longer time to enter anaphase from nuclear envelope breakdown, indicating a deficiency in reorganizing CCAN structure to achieve correct chromosome alignment in the absence of Ser299 phosphorylation. Statistical analyses confirmed that dynamic phosphorylation of Ser299 is required for accurate chromosome segregation (Figure 4C).

To test whether the mitotic arrest seen in CENP-N S299A-expressing cells is due to persistent activation of the spindle assembly checkpoint, the Mps1 inhibitor reversine was employed. As shown in Figure 4D (top panel), CENP-N S299A-expressing cells failed to enter anaphase even after 2 h of chromosome alignment. The addition of reversine prompted cells to enter anaphase in the presence of misaligned chromosomes, indicating that the spindle assembly checkpoint is activated in CENP-N S299A-expressing cells. Careful examination of the interface between CENP-L and CENP-N from the 3D structure indicated that CENP-N Ser299 and CENP-L Gln248 are in close contact (Figure 3E), suggesting that phosphorylation of Ser299 disrupts the interaction between CENP-L and CENP-N because of electrostatic repulsion and steric clash between phosphorylated Ser299 and Gln248. If CDK1-mediated CENP-N Ser299 phosphorylation regulates the dynamic interaction between CENP-N and CENP-L, then persistent phosphorylation of Ser299 would prevent CENP-L loading to the kinetochore. Consistent with this concept, expression of CENP-N S299D abolished the localization of CENP-L to the kinetochore (Supplementary Figure S3A). In addition, CENP-I failed to be localized to the kinetochore (Supplementary Figure S3B). However, cells expressing CENP-N S299D exhibited a distinct Nuf2 distribution (Supplementary Figure S3C), suggesting that the Ndc80 complex remains at the kinetochore despite CENP-N phosphorylation. Thus, phosphorylation of CENP-N Ser299 by CDK1 reorganizes CCAN for kinetochore plasticity and functions in accurate chromosome segregation.

CENP-N phosphorylation couples kinetochore remodeling to the spindle assembly checkpoint

CCAN controls kinetochore–microtubule interactions to achieve accurate metaphase alignment and error corrections in mitosis. To determine whether the checkpoint remains activated during the long-term arrest provoked by non-phosphorylatable CENP-N S299A, we used triple immunofluorescence to localize the checkpoint component Mad2 (Yao et al., 2000). Mad2 has been shown to preferentially bind to unattached kinetochores or to kinetochores that are attached but not under tension (Musacchio and Salmon, 2007). As shown in Figure 5A, in CENP-N S299A-expressing cells, high levels of kinetochore-associated Mad2 remained on lagging chromosomes (arrows and inset) but not on chromosomes near the spindle equator, while no kinetochore-associated Mad2 was observed on aligned chromosomes in wild-type CENP-N-expressing metaphase cells. Thus, the retention of Mad2 binding to kinetochores on lagging chromosomes indicates that impaired regulation of CENP-N phosphorylation prevents chromosome alignment and spindle assembly checkpoint silencing.

To test whether CENP-N phosphorylation-elicited reorganization of CCAN and its connectivity constitute the tension developed between sister kinetochores (inter-kinetochore), we measured the inter-kinetochore distance, which was identified by the peaks of Hec1 fluorescence spots. Our results showed that the inter-kinetochore distance was 1.28 ± 0.16 μm when the kinetochores were aligned in wild-type CENP-N-expressing cells but decreased to 1.01 ± 0.11 μm in cells expressing CENP-N S299A (Figure 5B). As a positive control, disruption of the CENP-L–CENP-N channel by TAT-peptide also reduced the inter-kinetochore distance to 0.97 ± 0.19 μm (Figure 5B). These results indicate that spindle microtubules fail to exert normal pulling forces on sister kinetochores when CENP-N phosphorylation is perturbed. Thus, we conclude that CDK1-elicited phosphorylation of CENP-N provides forces from kinetochore reorganization and spindle assembly checkpoint satisfaction to ensure accurate chromosome movements.

Discussion

The CCAN complex is composed of five subcomplexes, i.e. CENP-C, CENP-LN, CENP-OPQUR, CENP-HIKM, and CENP-TWSX. It is an essential kinetochore network and highly conserved across species, with a crucial role in kinetochore assembly and proper chromosome segregation during mitosis (Hori et al., 2008; Nishino et al., 2012; Takeuchi et al., 2014; Hinshaw and Harrison, 2019; Sedzro et al., 2022). Our study revealed an important regulatory interaction between CDK1 and the CENP-LN complex, which couples kinetochore reorganization and mitotic progression.

It has long been postulated that CCAN is only capable of binding to DNA once it is assembled into a complete protein machine (Cleveland et al., 2003; Cheeseman and Desai, 2008). Nonetheless, recent studies demonstrated that the assembly of CCAN is a stepwise process *in vitro* (Weir et al., 2016; Yan et al., 2019; Walstein et al., 2021). At an early stage in the cell cycle, the CENP-LN subcomplex binds exclusively to the centromere by recognizing the CENP-A L1 loop, potentially after CENP-A loads onto the centromere. In fact, phosphorylation of CENP-C by CDK1 in G2/M increases its competitive interaction with the CENP-A L1 loop (Ariyoshi et al., 2021), thus releasing the CENP-LN complex from CENP-A. Subsequently, CCAN rearranges to grab centromeric DNA for accurate chromosome alignment at metaphase and subsequent chromosome segregation (Figure 5C). Our structural and biochemical analyses of the CCAN complex, in combination with the data from previous reports (Weir et al., 2016; Tian et al., 2018; Yan et al., 2019; Walstein et al., 2021), suggest that the CCAN complex is dynamically assembled in a cell cycle-dependent manner governed by CDK1-mediated protein phosphorylation. To better

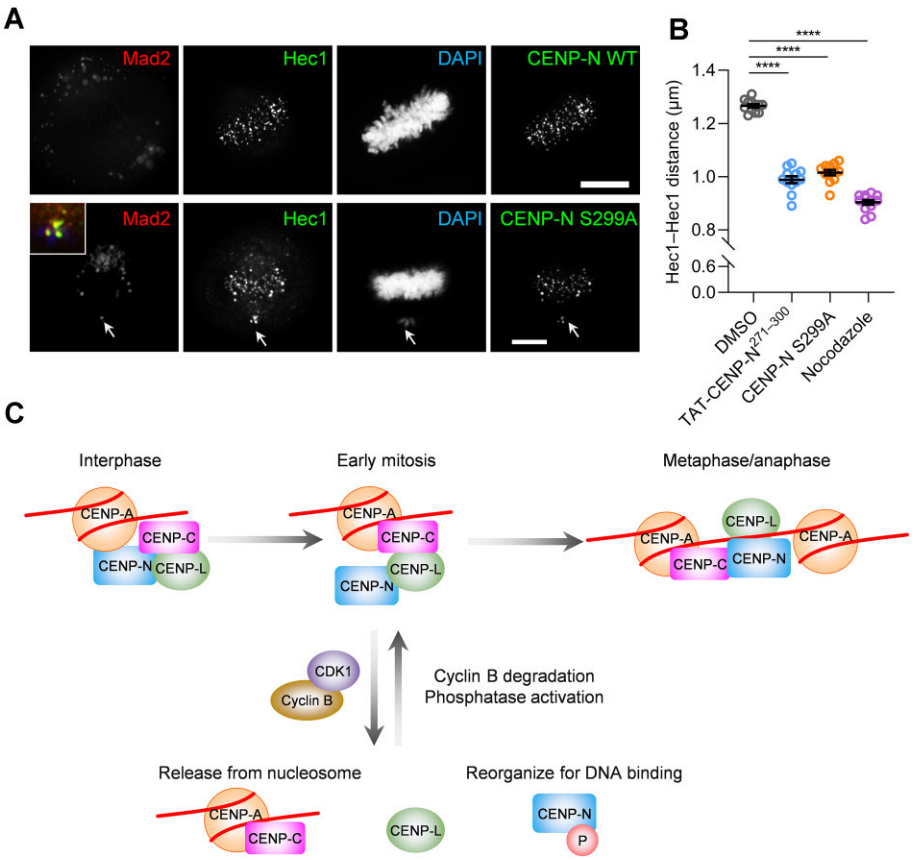

Figure 5 CENP-N phosphorylation couples kinetochore plasticity to CCAN mechano-sensitivity. (**A**) Immunofluorescence staining for the checkpoint protein Mad2 and the centromere marker Hec1 in cells expressing wild-type CENP-N or the CENP-N S299A mutant. In cells expressing the CENP-N S299A mutant (bottom panel), Mad2 labelling is restricted to chromosomes scattered near the poles. Scale bar, 10 μm. (**B**) Quantitation of the distance between sister kinetochores shown in **A**. The distance between sister kinetochores, as marked by Hec1 staining situated in the same focal plane, was determined using 100 kinetochores selected from at least 10 different cells. See 'Materials and methods' for details. (**C**) A working model illustrating the stepwise and dynamic assembly of CCAN to the centromere during the G1, S, and early G2 phases, resulting in the formation of a stable CENP-L–CENP-N channel required for the completion of CCAN assembly. Upon phosphorylation of CENP-N by CDK1, the CENP-L–CENP-N channel opens, allowing for the remodeling of CCAN and the binding of CENP-L–CENP-N to multiple sites on the centromeric DNA. This leads to tension development across sister kinetochores and within the same kinetochore, which is necessary for spindle assembly checkpoint satisfaction and accurate chromosome segregation.

understand the regulation of post-translational modification elicited by CDK1 on CCAN assembly, we generated a table to summarize the impact of CDK1-mediated phosphorylation on CCAN assembly and/or localization to the centromere (Supplementary Table S1).

Although exciting progress has been made toward a better understanding of the centromere architecture and the interdependence of centromere protein complexes (Weir et al., 2016; Yan et al., 2019; Walstein et al., 2021; Pesenti et al., 2022; Tian et al., 2022; Yatskevich et al., 2022), molecular mechanisms underlying dynamic CCAN assembly and their regulation during the cell cycle remain elusive. In this study, we identified CDK1 as a key regulator responsible for the dynamic assembly and precise remodeling of CCAN, which is essential for chromosome segregation. Early studies have discovered CENP-N as a CENP-A nucleosome reader and its assembly in early G1 (Jansen et al., 2007; Hori et al., 2008; McKinley et al., 2015). The N-terminal region of CENP-N is sufficient for specific recognition of the L1 loop of CENP-A in both budding yeast and humans (Pentakota et al., 2017; Chittori et al., 2018; Tian et al., 2018; Yan et al., 2019). However, little is known about whether the CENP-L–CENP-N interaction with CENP-A is regulated by post-translational modifications during the cell cycle.

During the preparation of revision to this article, Navarro and Cheeseman (2022) reported that the recruitment of the CENP-LN complex to the centromere is regulated by cell cycle-dependent phosphorylation. Using site-directed mutagenesis coupled with immunofluorescence microscopic analyses, they revealed that CENP-N phosphorylation by CDK1 regulates CENP-N localization at the centromere, which supports our finding. We compared

and contrasted CENP-N phosphorylation sites identified in these two studies (Supplementary Table S2). In our study, we demonstrated that Ser299 is a key phosphorylation site whose phosphorylation is sufficient to perturb the CENP-L–CENP-N interaction. Since both phospho-mimicking and non-phosphorylatable CENP-N Ser299 mutants result in mitotic abnormalities, we performed an immunoprecipitation–mass spectrometry analysis to identify the differential mitotic binding partners that may account for the phenotypes (Supplementary Table S3). Although the mutation at Thr273, similar to Ser299, disrupts the formation of the CENP-LN complex and the recruitment of CENP-N to the centromere, the adjacent sequence of Thr273 does not conform to the CDK1 substrate consensus (pS/pT-[P]; pS/pT-[P]-X-R). Moreover, we were unable to detect phosphorylation of CENP-N Thr273 *in vitro* or in mitotic cells. Therefore, we conclude that the reduced binding of CENP-N T273D to CENP-L is due to the electrostatic property of Thr273 rather than phosphorylation. It is worth noting that Navarro and Cheeseman (2022) discovered that phosphorylation of CENP-L by CDK1 also regulates the recruitment of the CENP-LN complex and chromosome segregation in mitosis. It will be of great interest to ascertain the respective phosphorylation status of CENP-L and CENP-N during the cell cycle and their respective functional specificities.

Interestingly, the recombinant CENP-N protein was not phosphorylated by CDK1 *in vitro*, as the tight CENP-L–CENP-N interaction prevents the access of CDK1 to Ser299 due to steric hindrance of CENP-L binding, suggesting that the release of CENP-L–CENP-N dimerization occurs prior to CDK1-mediated phosphorylation during the cell cycle. The spatiotemporal regulation of the CENP-L–CENP-N association by CDK1 during the cell cycle revealed in this study provides mechanistic insights into the molecular delineation of dynamic kinetochore architecture remodeling in mitosis (Figure 5C). The excitement and challenge ahead are to employ single-molecule analyses to visualize the conformational flexibility of the CENP-L–CENP-N channel and tie this to the mechanism of action underlying spindle assembly checkpoint satisfaction in living mitotic cells. In addition, it would be equally important to identify all CDK1-regulated phosphorylation sites on CCAN for modeling CCAN reorganization during the cell cycle. Future analyses of the CCAN–CENP-A nucleosome complex structure and composition using proximity ligation proteomics and the *in situ* structure of chromatin–kinetochore–microtubules using cryo-correlative light and electron microscopy will be helpful to delineate mechanisms of action underlying CCAN reorganization during mitosis.

Taken together, we propose that the phospho-regulation of CENP-N by CDK1 establishes dynamic centromere–kinetochore interactions by reorganizing outer kinetochore proteins and enabling accurate kinetochore–microtubule attachment. It is likely that all the CCAN–KMN network proteins interact to orchestrate a functional kinetochore during chromosome segregation. The CDK1–CENP-N interaction established here is a core of this giant and dynamic complex, which orchestrates kinetochore core complex assembly to spindle microtubule attachment in the centromere.

Materials and methods

Plasmids

To generate GFP-tagged CENP-N, PCR-amplified CENP-N cDNA was cloned into the pEGFP-C1 and pLVX-EGFP-C1 vectors by the ClonExpress Entry One Step Cloning Kit (Vazyme). To generate FLAG-tagged CENP-N and CENP-L, PCR-amplified CENP-N and CENP-L cDNAs were cloned into the 3×FLAG-Myc-CMV-24 vector by the ClonExpress Entry One Step Cloning Kit (Vazyme). Site-specific mutants (T273A, T273D, S299A, S299D, S320A, and S320D) of CENP-N were generated by Mut Express II Fast Mutagenesis Kits (Vazyme). All plasmids with the desired insertions and mutations were sequenced at General Biosystems.

Cell culture, synchronization, and transfection

HeLa and HEK293T cells were maintained in Dulbecco's modified Eagle's medium (DMEM, Gibco) with 10% fetal bovine serum (FBS, Hyclone) and 100 units/ml penicillin (Gibco) plus 100 μg/ml streptomycin (Gibco). The inducible CRISPR/Cas9-mediated endogenous CENP-N knockout HeLa cells from Dr Iain Cheeseman's laboratory were maintained in DMEM (Gibco) supplemented with 10% FBS (Tet-tested, Atlanta Biologicals), 100 units/ml penicillin (Gibco), 100 μg/ml streptomycin (Gibco), 50 μg/ml G418 (Sigma), and 2.5 μg/ml puromycin (Sigma). Doxycycline (1 μg/ml, Sigma) was used to induce CENP-N knockout (McKinley and Cheeseman, 2017). Cells were synchronized to mitosis by thymidine or MG132 release before real-time imaging as reported (Mo et al., 2016; Bao et al., 2018). Transfection of plasmids and shRNAs into cells was performed with Lipofectamine 3000 (Invitrogen) according to the user's manual.

For rescue experiments, inducible CRISPR/Cas9-mediated endogenous CENP-N knockout HeLa cells were infected with lentiviruses expressing sgRNA-resistant GFP-tagged CENP-N protein (wild-type, S299A, or S299D). Cell lines stably expressing wild-type CENP-N, CENP-N S299A, or CENP-N S299D were isolated by single-cell sorting (BD LSRFortessa).

Drug treatment

Thymidine (T9250, 2 mM), Ro3306 (SML0569, 10 μM), reversine (R3904, 500 nM), and MG132 (C2211, 20 μM) were from Sigma. Puromycin was from Thermo (A1113802).

Antibodies

For immunofluorescence, anti-CENP-I (rabbit, Cell Signaling Technology, 49426), anti-Nuf2 (Abcam, ab122962), ACA (Immunovision, HCT-0100), anti-HEC1 (Abcam, ab3613), anti-CENP-L (kindly gifted by Dr Iain Cheeseman), and anti-CENP-N (kindly gifted by Dr Iain Cheeseman) antibodies were used. For western blotting, anti-α-tubulin (mouse, DM1A, Sigma, 05-829, 1:5000), anti-β-actin (Servicebio, GB12001), anti-Cyclin B1 (rabbit, Cell Signaling Technology, 12231, 1:1000), anti-FLAG (Sigma, F1804, 1:2000), anti-GFP (Proteintech, 50430-2-AP, 1:1000), and anti-CENP-N (Affinity Biosciences, DF2315, 1:500) antibodies were used. The appropriate secondary antibodies were purchased from Jackson ImmunoResearch Laboratories.

To generate anti-CENP-N phospho-Ser299 (pS299) antibody, a synthetic peptide containing phosphorylated Ser299 (LIKFS-*p*S-PHLLEALC) was conjugated to rabbit albumin (Sigma) and immunized into rabbits as described (Huang et al., 2019). The serum was collected by a standard protocol and preabsorbed by a non-phosphorylated CENP-N peptide (LIKFSPHLLEALC) followed by affinity purification using (LIKFS-*p*S-PHLLEALC)-conjugated sulfone Sepharose beads. The CENP-N pS299 site-specific antibodies were characterized according to standard procedures (Xia et al., 2012; Mo et al., 2016).

Kinase assay

Kinase reactions were performed in 40 μl of kinase buffer (25 mM HEPES, pH 7.2, 50 mM NaCl, 2 mM EGTA, 5 mM $MgSO_4$, 1 mM DTT, and 0.01% Brij35) with 3× FLAG-CENP-N (2 μg) as substrate, 100 ng of purified CDK1 (Thermo, PV3292) as kinase, 5 μCi [γ-^{32}P]-ATP, and 500 μM ATP as described previously (Xia et al., 2012; Mo et al., 2016; Huang et al., 2019). The reaction mixtures were incubated at 30°C for 30 min and then terminated by 5× SDS–PAGE loading buffer (10% SDS, 0.5% bromophenol blue, 50% glycerol, and 100 mM DTT). After the samples were boiled at 100°C for 2 min, 50% of the sample was resolved by SDS–PAGE and stained by Coomassie brilliant blue (CBB) R250. For autoradiograms, CBB-stained gels were destained, scanned, and dried between sheets of cellulose for 4 h. The semi-dried gels were then placed between an intensifier and X-ray film for 12–24 h in a −80°C freezer, and the incorporation of ^{32}P into CENP-N proteins was quantified by PhosphorImager (Amersham Biosciences).

Immunofluorescence microscopy, image processing, and quantification

HeLa cells grown on coverslips were fixed and permeabilized simultaneously with PTEMF buffer (50 mM Pipes, pH 6.8, 0.2% Triton X-100, 10 mM EGTA, 1 mM $MgCl_2$, and 4% formaldehyde) at room temperature and were processed for indirect immunofluorescence microscopy. Samples were examined on a DeltaVision microscope (Applied Precision) with a 60× objective lens, NA = 1.42, with optical sections acquired 0.25 μm apart on the z axis. Deconvoluted images from each focal plane were projected into a single picture using Softworx (Applied Precision). Images were taken at identical exposure times within each experiment and acquired as 16-bit gray-scale images. After deconvolution, the images were exported as 24-bit RGB images and processed in Adobe Photoshop. Images shown in the same panel have been identically scaled. Kinetochore intensities were measured in ImageJ (rsb.info.nih.gov/ij/) on non-deconvoluted images. The levels of kinetochore-associated proteins were quantified as described previously (Dou et al., 2015). In brief, the average pixel intensities from at least 100 kinetochore pairs from five cells were measured, and background pixel intensities were subtracted. The pixel intensities at each kinetochore pair were then normalized against ACA pixel values to account for any variations in staining or image acquisition. Unless otherwise specified, the values for treated cells were then plotted as a percentage of the values obtained from cells of the control groups.

Time-lapse imaging

For time-lapse imaging, HeLa cells were cultured in glass-bottom culture dishes (MatTek) and maintained in CO_2-independent medium (Gibco) supplemented with 10% FBS and 2 mM glutamine. During imaging, the dishes were placed in a sealed chamber at 37°C. Images of living cells were taken with the DeltaVision microscopy system. For presenting details of the real-time imaging, projection images were constructed from 0.5 μm/section for three sections within a cell.

TAT-CENP-N$^{271-300}$ peptide treatment

To directly assess the functional effect of the CENP-N–CENP-L interaction on mitosis, a membrane-permeable peptide containing CENP-N (aa 271–300) was commercially synthesized (named TAT-CENP-N$^{271-300}$ peptide, 5′-YGRKKRRQRRR-GGSGG-LETKFKSGLN-GSILAEREEP-LRCLIKFSSP-3′). Trial experiments were employed to determine the optimal concentration of the peptide to perturb the CENP-N–CENP-L interaction in HeLa cells, which was identified at 5 μM. mCherry-H2B-expressing HeLa cells were cultured to 50%–60% confluency before thymidine synchronization. Then, the cells were washed with serum-free Opti-MEM media and immediately incubated with TAT-CENP-N$^{271-300}$ peptide at 5 μM for 30 min. After incubation, cells were washed with phosphate-buffered saline, maintained in CO_2-independent medium, and directly examined by live cell imaging. Cells exhibiting unaligned chromosomes that failed to align at the metaphase plate within 90 min after nuclear envelope breakdown were considered to undergo mitotic arrest.

Immunoprecipitation

For immunoprecipitation, cells were treated with scramble peptide or TAT-CENP-N$^{271-300}$ peptide for 1 h in Opti-MEM medium (Thermo), collected, and lysed in HEPES buffer (20 mM HEPES, pH 7.4, 150 mM NaCl, 1 mM EDTA, and 0.1% Triton X-100) supplemented with protease inhibitor cocktail (Sigma) and phosphatase inhibitor cocktail (Sigma). After pre-clearing with protein A/G resin, cell lysates were incubated with anti-CENP-L antibodies at 4°C for 2 h with gentle rotation. Protein A/G resin was added to the lysates and incubated for another 2 h. Protein A/G resin was then spun down and washed five times with lysis buffer before being resolved by SDS–PAGE and immunoblotted with the indicated antibodies.

For FLAG-tagged protein immunoprecipitation, transfected cells were collected and lysed in lysis buffer (20 mM HEPES, pH 7.4, 150 mM NaCl, 1 mM EDTA, and 0.1% Triton X-100) supplemented with protease inhibitor cocktail (Sigma), as previously reported (Song et al., 2021). Cell lysates were clarified by centrifugation and incubated with FLAG-M2 resin (Sigma) at 4°C with gentle rotation. After washing three times with lysis buffer, the FLAG beads were boiled and assessed by western blotting.

Mass spectrometry sample preparation and phosphorylation site analysis

HeLa cells were transfected with 3× FLAG-CENP-N plasmids using Lipofectamine 3000 (Invitrogen) for 12 h and then blocked at mitosis with 100 ng/mL nocodazole (Sigma-Aldrich) for 16 h. Cells were treated with the CDK1 inhibitor Ro3306 (5 μM) for another 1 h and subjected to FLAG-tagged protein immunoprecipitation. After washing, the samples were reduced with 10 mM DTT in 50 mM ammonium bicarbonate at 56°C for 30 min and then alkylated with 30 mM iodoacetamide for 30 min. Afterwards, 2 μg of trypsin (Promega, V511A) was added to the samples for overnight digestion at 37°C. After trypsin digestion, the peptide samples were desalted and analyzed with a Thermo Fisher Q Exactive mass spectrometer equipped with Easy-nanoLC 1200, followed by a scan range of m/z 350–1550. The raw files were analyzed with pFind 2.8. Phosphorylation (S/T, +79.9663 Da) and oxidation (M, +15.9949 Da) modifications were included as variable modifications. Carbamidomethyl (C, +57.0215 Da) was set as a fixed modification.

Structural modeling of phosphorylation of CENP-N Ser299

The experimental cryo-EM structure of the CCAN complex (PDBID: 7XHO) was used to examine the binding interface between CENP-L and CENP-N. To model phosphorylation of CENP-N Ser299, we used *Get Monomer molecule* in *COOT* to generate coordinates from the REFMAC monomer library by inputting 'SEP', which is a letter code indicating phosphorylserine. The following steps were performed: (i) replacing CENP-N Ser299 with pS299 and generating a new PDB file, (ii) opening the new PDB with a text file and moving the coordinate of pS299 to the correct position, and (iii) refining the modified PDB file in *COOT* with *real_space_refine*.

Statistics and reproducibility

All experiments were performed three times independently with similar results. Statistical analyses were performed with GraphPad Prism 8. No statistical method was used to predetermine the sample size. Images were mounted in figures using Photoshop (Adobe).

Supplementary material

Supplementary material is available at *Journal of Molecular Cell Biology* online.

Acknowledgements

We are grateful to Drs Iain Cheeseman (Whitehead Institute for Biomedical Research) and Andrea Musacchio (Max Planck Institute of Molecular Physiology) for reagents and suggestions.

Funding

This work was supported by grants from the Ministry of Science and Technology of the People's Republic of China and the National Natural Science Foundation of China (2022YFA1303100, 2022YFA0806800, 92153302, 32090040, 92254302, 21922706, and 91853115 to X.L.; 2017YFA0503600, 31621002, U1532109, and 91853133 to J.Z.; 32170733, 2017YFA0102900, and 31871359 to Z.D.; 32000858 to T.T.), the Strategic Priority Research Program of the Chinese Academy of Sciences (XDB37010105 to J.Z. and XDB19040000 to X.L.), the Ministry of Education (IRT_17R102, 20113402130010, and YD2070006001 to X.L.), Anhui Provincial Natural Science Foundation (2108085J15 to Z.D.; 2008085QC145 to T.T.), the Fundamental Research Funds for the Central Universities (WK2070000171 to T.T.), and the University of Science and Technology of China Research Funds of the Double First-Class Initiative (YD2070002015 to X.Z.). The funders had no role in the study design, data collection and analysis, decision to publish, or preparation of the manuscript.

Conflict of interest: none declared.

Author contributions: X. Yao and X.L. conceived the project. R.L., Z.D., P.G., X.G., X. Yuan, M.M., and F.A. designed and performed most of the biochemical and cell biological experiments. T.T. and L.C. assisted in molecular modeling and recombinant protein engineering. L.N., G.B., and P.Z. contributed reagents. R.L., T.T., C.W., X.Z., Z.D., and X. Yuan analyzed data. X.L., Z.D., R.L., J.Z., and X. Yao wrote the manuscript. All authors have commented and approved the manuscript.

References

Ariyoshi, M., Makino, F., Watanabe, R., et al. (2021). Cryo-EM structure of the CENP-A nucleosome in complex with phosphorylated CENP-C. EMBO J. *40*, e105671.

Bao, X., Liu, H., Liu, X., et al. (2018). Mitosis-specific acetylation tunes Ran effector binding for chromosome segregation. J. Mol. Cell Biol. *10*, 18–32.

Carroll, C.W., Silva, M.C., Godek, K.M., et al. (2009). Centromere assembly requires the direct recognition of CENP-A nucleosomes by CENP-N. Nat. Cell Biol. *11*, 896–902.

Cheeseman, I.M., and Desai, A. (2008). Molecular architecture of the kinetochore–microtubule interface. Nat. Rev. Mol. Cell Biol. *9*, 33–46.

Chittori, S., Hong, J., Saunders, H., et al. (2018). Structural mechanisms of centromeric nucleosome recognition by the kinetochore protein CENP-N. Science *359*, 339–343.

Cleveland, D.W., Mao, Y., and Sullivan, K.F. (2003). Centromeres and kinetochores: from epigenetics to mitotic checkpoint signaling. Cell *112*, 407–421.

Dou, Z., Liu, X., Wang, W., et al. (2015). Dynamic localization of Mps1 kinase to kinetochores is essential for accurate spindle microtubule attachment. Proc. Natl Acad. Sci. USA *112*, E4546–E4555.

Dou, Z., Prifti, D.K., Gui, P., et al. (2019). Recent progress on the localization of the spindle assembly checkpoint machinery to kinetochores. Cells *8*, 278.

Fang, J., Liu, Y., Wei, Y., et al. (2015). Structural transitions of centromeric chromatin regulate the cell cycle-dependent recruitment of CENP-N. Genes Dev. *29*, 1058–1073.

Foltz, D.R., Jansen, L.E., Black, B.E., et al. (2006). The human CENP-A centromeric nucleosome-associated complex. Nat. Cell Biol. *8*, 458–469.

Hara, M., Ariyoshi, M., Okumura, E.I., et al. (2018). Multiple phosphorylations control recruitment of the KMN network onto kinetochores. Nat. Cell Biol. *20*, 1378–1388.

Hellwig, D., Emmerth, S., Ulbricht, T., et al. (2011). Dynamics of CENP-N kinetochore binding during the cell cycle. J. Cell Sci. *124*, 3871–3883.

Hinshaw, S.M., and Harrison, S.C. (2019). The structure of the Ctf19c/CCAN from budding yeast. eLife *8*, e44239.

Hori, T., Amano, M., Suzuki, A., et al. (2008). CCAN makes multiple contacts with centromeric DNA to provide distinct pathways to the outer kinetochore. Cell *135*, 1039–1052.

Huang, Y., Lin, L., Liu, X., et al. (2019). BubR1 phosphorylates CENP-E as a switch enabling the transition from lateral association to end-on capture of spindle microtubules. Cell Res. *29*, 562–578.

Jansen, L.E., Black, B.E., Foltz, D.R., et al. (2007). Propagation of centromeric chromatin requires exit from mitosis. J. Cell Biol. *176*, 795–805.

Liu, X., Wang, H., Dou, Z., et al. (2020). Phase separation drives decision making in cell division. J. Biol. Chem. *295*, 13419–13431.

McKinley, K.L., and Cheeseman, I.M. (2016). The molecular basis for centromere identity and function. Nat. Rev. Mol. Cell Biol. *17*, 16–29.

McKinley, K.L., and Cheeseman, I.M. (2017). Large-scale analysis of CRISPR/Cas9 cell-cycle knockouts reveals the diversity of p53-dependent responses to cell-cycle defects. Dev. Cell *40*, 405–420.e2.

McKinley, K.L., Sekulic, N., Guo, L.Y., et al. (2015). The CENP-L-N complex forms a critical node in an integrated meshwork of interactions at the centromere–kinetochore interface. Mol. Cell *60*, 886–898.

Mo, F., Zhuang, X., Liu, X., et al. (2016). Acetylation of Aurora B by TIP60 ensures accurate chromosomal segregation. Nat. Chem. Biol. *12*, 226–232.

Musacchio, A., and Desai, A. (2017). A molecular view of kinetochore assembly and function. Biology *6*, 5.

Musacchio, A., and Salmon, E.D. (2007). The spindle-assembly checkpoint in space and time. Nat. Rev. Mol. Cell Biol. *8*, 379–393.

Navarro, A.P., and Cheeseman, I.M. (2022). Dynamic cell cycle-dependent phosphorylation modulates CENP-L–CENP-N centromere recruitment. Mol. Biol. Cell *33*, ar87.

Nishino, T., Takeuchi, K., Gascoigne, K.E., et al. (2012). CENP-T–W–S–X forms a unique centromeric chromatin structure with a histone-like fold. Cell *148*, 487–501.

Okada, M., Cheeseman, I.M., Hori, T., et al. (2006). The CENP-H-I complex is required for the efficient incorporation of newly synthesized CENP-A into centromeres. Nat. Cell Biol. *8*, 446–457.

Pentakota, S., Zhou, K., Smith, C., et al. (2017). Decoding the centromeric nucleosome through CENP-N. eLife *6*, e33442.

Pesenti, M.E., Raisch, T., Conti, D., et al. (2022). Structure of the human inner kinetochore CCAN complex and its significance for human centromere organization. Mol. Cell *82*, 2113–2131.e8.

Schleiffer, A., Maier, M., Litos, G., et al. (2012). CENP-T proteins are conserved centromere receptors of the Ndc80 complex. Nat. Cell Biol. *14*, 604–613.

Sedzro, D.M., Yuan, X., Mullen, M., et al. (2022). Phosphorylation of CENP-R by Aurora B regulates kinetochore–microtubule attachment for accurate chromosome segregation. J. Mol. Cell Biol. *14*, mjac051.

Song, X., Yang, F., Liu, X., et al. (2021). Dynamic crotonylation of EB1 by TIP60 ensures accurate spindle positioning in mitosis. Nat. Chem. Biol. *17*, 1314–1323.

Takeuchi, K., Nishino, T., Mayanagi, K., et al. (2014). The centromeric nucleosome-like CENP-T–W–S–X complex induces positive supercoils into DNA. Nucleic Acids Res. *42*, 1644–1655.

Tian, T., Chen, L., Dou, Z., et al. (2022). Structural insights into human CCAN complex assembled onto DNA. Cell Discov. *8*, 90.

Tian, T., Li, X., Liu, Y., et al. (2018). Molecular basis for CENP-N recognition of CENP-A nucleosome on the human kinetochore. Cell Res. *28*, 374–378.

Walstein, K., Petrovic, A., Pan, D., et al. (2021). Assembly principles and stoichiometry of a complete human kinetochore module. Sci. Adv. *7*, eabg1037.

Weir, J.R., Faesen, A.C., Klare, K., et al. (2016). Insights from biochemical reconstitution into the architecture of human kinetochores. Nature *537*, 249–253.

Xia, P., Wang, Z., Liu, X., et al. (2012). EB1 acetylation by P300/CBP-associated factor (PCAF) ensures accurate kinetochore–microtubule interactions in mitosis. Proc. Natl Acad. Sci. USA *109*, 16564–16569.

Yan, K., Yang, J., Zhang, Z., et al. (2019). Structure of the inner kinetochore CCAN complex assembled onto a centromeric nucleosome. Nature *574*, 278–282.

Yao, X., Abrieu, A., Zheng, Y., et al. (2000). CENP-E forms a link between attachment of spindle microtubules to kinetochores and the mitotic checkpoint. Nat. Cell Biol. *2*, 484–491.

Yao, X., Anderson, K.L., and Cleveland, D.W. (1997). The microtubule-dependent motor centromere-associated protein E (CENP-E) is an integral component of kinetochore corona fibers that link centromeres to spindle microtubules. J. Cell Biol. *139*, 435–447.

Yatskevich, S., Muir, K.W., Bellini, D., et al. (2022). Structure of the human inner kinetochore bound to a centromeric CENP-A nucleosome. Science *376*, 844–852.

Received July 26, 2022. Revised January 9, 2023. Accepted June 24, 2023.